

## Revealing atomic-scale vacancy-solute interaction in nickel

Felipe F. Morgado<sup>1,\*</sup>, Shyam Katnagallu<sup>1,2</sup>, Christoph Freysoldt<sup>3</sup>, Benjamin Klaes<sup>4</sup>, François Vurpillot<sup>1,4</sup>, Jörg Neugebauer<sup>3</sup>, Dierk Raabe<sup>1</sup>, Steffen Neumeier<sup>5</sup>, Baptiste Gault<sup>1,6,‡</sup> and Leigh T. Stephenson<sup>1,‡</sup>

<sup>1</sup>Max-Planck-Institut für Eisenforschung, Max-Planck-Str. 1, 40237, Düsseldorf, Germany

<sup>2</sup>now at Karlsruhe Institut für Technologie (north campus), Hermann-von-Helmholtz-platz 1, 76344, Eggenstein-Leopoldshafen, Germany

<sup>3</sup>Department of Computational Materials Design, Max-Planck-Institut für Eisenforschung GmbH, Düsseldorf, Germany

<sup>4</sup>Groupe Physique des Matériaux, Université de Rouen, Saint Etienne du Rouvray, Normandie 76800, France

<sup>5</sup>Materials Science and Engineering, Institute 1, Friedrich-Alexander-Universität Erlangen-Nürnberg, Erlangen, Germany

<sup>6</sup>Department of Materials, Royal School of Mines, Imperial College London, London, SW7 2AZ, UK

(Received 02 March 2021;)

Imaging individual vacancies in solids and revealing their interactions with solute atoms remains one of the frontiers in microscopy and microanalysis. Here we study a creep-deformed binary Ni-2 at.% Ta alloy. Atom probe tomography reveals a random distribution of Ta. Field ion microscopy, with contrast interpretation supported by density-functional theory and time-of-flight mass spectrometry, evidences a positive correlation of tantalum with vacancies. Our results support solute-vacancy binding, which explains improvement in creep resistance of Ta-containing Ni-based superalloys and helps guide future material design strategies.

Understanding a material's properties requires comprehensive knowledge of the atomic-scale arrangement of the constituting elements [1], particularly their interactions with crystalline defects, including interfaces [2], dislocation [3], and vacancies [4]. Field ion microscopy (FIM), the predecessor to atom probe tomography (APT), is likely the only technique allowing for imaging materials in three-dimensions with true atomic-resolution.

FIM was developed in the 1950s and was the first technique to image individual atoms at a metal surface [5]. Through field ionization of an imaging gas near the sharp needle specimen's surface, FIM provides an atomically-resolved projection of the surface with near 100% imaging efficiency. FIM gives critical information regarding crystallographic defects such as vacancies [6, 7, 8, 9], dislocations [10, 11, 12], or grain boundaries [12, 13]. However, the nature of the contrast in FIM is still a matter of debate [14], making single atomic-scale studies of solute-defect interactions challenging. There is a difference in FIM contrast caused, on the one hand, by different chemical elements and, on the other hand, by different local curvatures (i.e., electric fields) [15]. The ability to distinguish between these contributions is still debated. Analytical FIM (AFIM) was proposed to tackle this problem [16], taking an example in a Ni-Re binary alloy, used as a solid solution model substance to a nickel-based superalloy.

Superalloys are critical engineering materials for load-bearing applications at high-temperature in harsh gaseous environments, enabling turbines for air traffic or large-scale energy conversion [17, 18, 19]. More specifically, single crystals are used in the most demanding

environments to avoid failure by damage accumulation at grain boundaries [20, 21]. Numerous studies have focused on understanding the deformation mechanisms, particularly for creep [22, 23, 24]. At high temperatures, creep occurs mainly through dislocation slip and dislocation climb [25, 26]. The latter consists of the emission or absorption of vacancies by the core of an edge dislocation that will climb in the normal direction to its glide plane. Therefore, understanding solute-vacancy interaction is critical for predicting and potentially enhancing creep lifetime.

Re is the best solid solution strengthening element in Ni-based superalloys at high temperatures [27], but other elements give a better solid solution strengthening effect at lower temperatures. Also, Re is an expensive and rare element and, depending on the alloy, can represent half the cost of the raw material to produce a turbine blade [28]. APT, complemented by transmission electron microscopy and atomistic simulations, helped reveal that Re extends creep lifetime by imposing a drag force that slows down the climbing dislocations [29]. Tantalum provides the most significant strengthening at lower temperatures [30], although it has to be taken into account that Ta partitions predominantly to the precipitate phase in Ni-based superalloys. In addition to the large atomic size of Ta, simulation suggests that there is an attractive interaction between the tantalum atoms and vacancies [31]. Yet this has not been experimentally proven.

Here, we characterize a creep-deformed binary Ni-2 at.% Ta alloy using APT and AFIM. APT analysis reveals a random distribution of Ta within the Ni matrix. AFIM allows to image vacancies located in the first nearest-neighbor position to Ta atoms. An investigation related to

the FIM contrast, supported by DFT calculations and AFIM experiments, is also presented. This combined set of experiments and theory helps rationalize the previously-proposed mechanism underpinning the increase in superalloys' lifetime in high temperature applications by Ta-addition.

All details regarding the preparation of the alloy can be found in ref. [30]. A solid solution single crystal alloy of Ni-2 at.% Ta was cast. A cylindrical specimen was subjected to a uniaxial compression at 1050 °C using a pneumatic compression creep testing machine at a constant applied stress of 20 MPa until a plastic strain of about 11 % was reached within 2.9 h.

Needle-shaped specimens suitable for APT and FIM were prepared at the FEI Helios PFIB, which uses a xenon plasma ion source instead of the more common gallium source. The preparation procedure is discussed in [32]. Both APT and FIM measurements were performed on a LEAPTM 5000 XS (Cameca Instruments). The APT measurements were conducted in voltage pulsing mode using a pulse fraction of 20%, a pulse repetition rate of 200 kHz, a temperature of 40 K, and a detection rate of 0.5 %. APT data processing and reconstruction were performed using the commercial software IVAS 3.8.4. The FIM measurements were done with a 99.999% purity neon as imaging gas via a manually controlled leak valve. The pressure in the analysis chamber was maintained at approximately  $1 \times 10^{-6}$  mbar. The AFIM technique was performed using the APT in-situ time-of-flight mass spectrometer by superimposing a pulsed voltage on the DC voltage (pulse fraction of 20%) at the FIM working pressure. The data is extracted as an EPOS file and processed using in-house built routines within MATLAB R2019a.

We first used APT to confirm the composition of the alloy and assess the Ta-distribution. Figure 1(a) is the tomographic reconstruction showing the Ni and Ta atoms in purple and green, respectively. The composition found was Ni 97.9 and Ta 2.1 at.%, which is very close to the nominal composition. Figure 1(b) shows the distribution of distance to the first-nearest neighbor Ta atom within the reconstructed APT point cloud, along with a corresponding random distribution [33]. No clustering is observed.

Figure 2(a) shows a field ion micrograph of the crept sample. The image reveals the symmetries associated with the alloy's face-centered cubic structure, and, in some of the atomic terraces, a true atomic resolution is achieved. The enlarged region corresponds to the (012) atomic planes. As we increase the voltage, the field evaporation of the surface atoms allows us to image deeper layers within the material. Figure 2(b)-(e) shows the successive atomic planes as the topmost layers are removed nearly atom-by-atom. Some atoms are imaged larger and brighter than others. A vacancy is observed underneath one of the

brighter atoms and can be seen clearly after a few atoms are field evaporated in Figure 2(e). The creep deformation proceeds by the emission of many point defects. Although, imaging these vacancies would be very unlikely (typical concentration of  $10^{-7}$  vacancy/atom) [34]. What we imaged here are the vacancies associated with the brighter atoms. This observation was made on multiple occasions – see supplementary information. The micrograph in Fig. S1 was obtained using conventional field-ion microscope. Given the field evaporation sequence, the observed vacancy could be an artifact created by the field evaporation of the brighter atom, as reported by Stiller et al. [35]. Fig. S2 confirms the presence of vacancies as a vacancy is observed in the plane above the brighter atom.

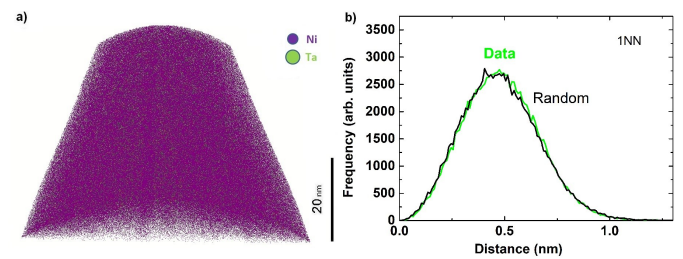


Figure 1: Atom probe tomography measurement of the crept sample. a) Reconstruction of the deformed sample. b) First nearest neighbor distribution between tantalum atoms.

To interpret the brightness contrast between Ni and Ta, we investigated the geometric and electronic structure of the Ni (012) surface by using density functional theory (DFT) calculations in the presence of an electric field of 40 V/nm. DFT was performed in the plane-wave PAW formalism with the SPHInX code [36] using the Perdew-Burke-Ernzerhof (PBE) exchange-correlation functional with D2 van-der-Waals corrections, which allowed us to investigate the interaction with Ne adatoms. The plane-wave cutoff was 20 Ry. The Ni (012) surface was modeled in the repeated slab approach with 9 atomic layers at the theoretical lattice constant (3.465Å). Finite electric fields of 40 V/nm were introduced with the generalized dipole correction [37]. Tantalum substitution at the surface was modeled in a  $3 \times 3$  surface unit cell, employing a  $2 \times 3 \times 1$  offset  $\mathbf{k}$ -point sampling ( $4 \times 6 \times 1$  for DOS calculations). Calculations including a Ne-adlayer did not show any notable influence.

Due to the electrostatic field, the surface becomes charged by 0.3 atomic charge units (e) per surface atom. Using Hirshfeld decomposition to assign the charges to individual atoms, we find that the surface charge on this relatively open surface is located 90% on the top-layer atoms, and 10% on the second layer. Substitutional Ta relaxes outward compared to the surrounding Ni atoms by  $\approx 0.1 \text{ \AA}$  due to its slightly larger atomic size, but acquires a significantly higher charge (0.6e), which is transferred from the other eight top-surface atoms (in total: 0.15e)

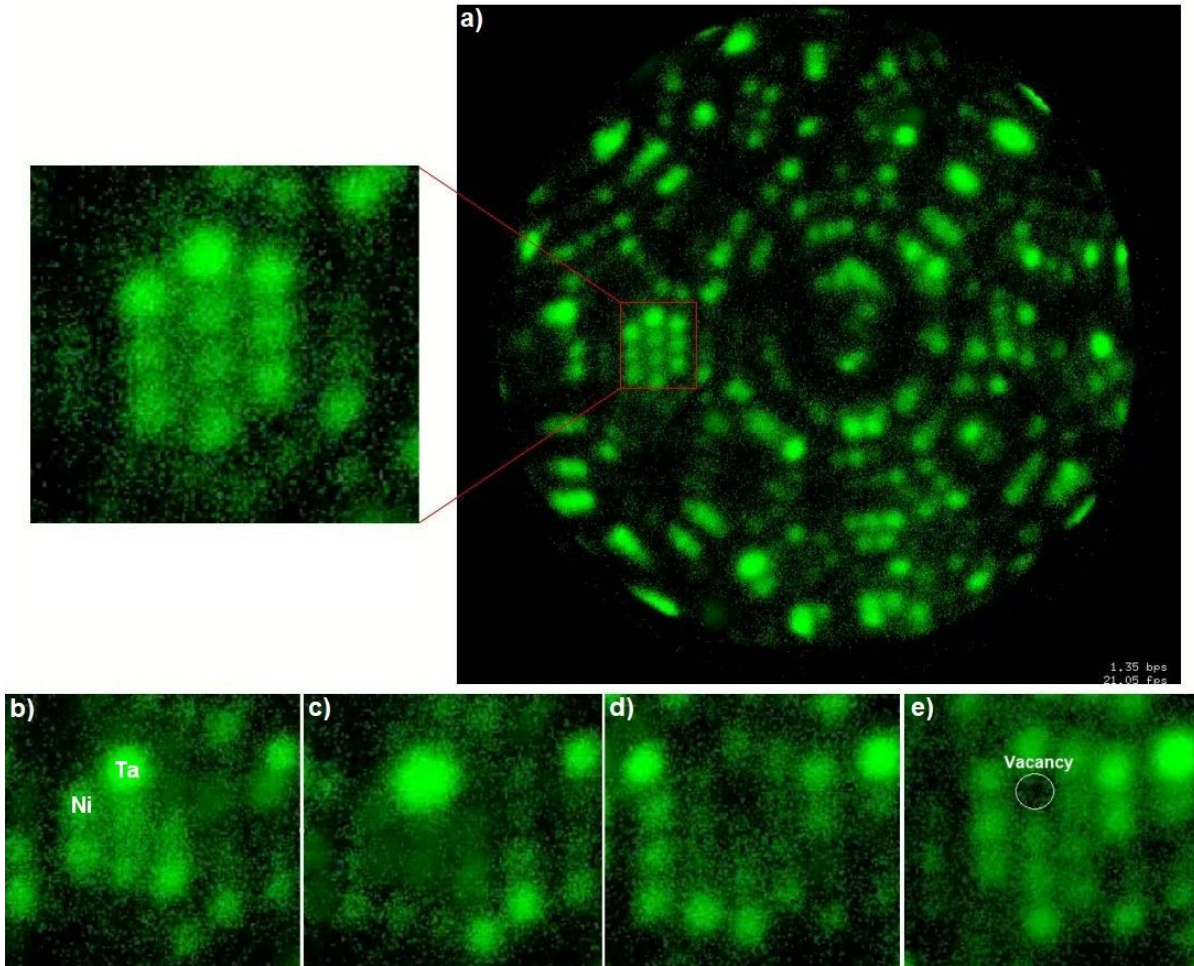


Figure 2: Field ion microscopy measurement. (a) Field ion micrograph zoomed on the (012) planes. (b)-(e) shows consecutively atomic layers.

and the three second-layer atoms directly below Ta (0.14e). The increased local electrostatic field likely affects the probability of tunneling from the Ne p-electrons into the surface, but it also enhances the local concentration of imaging gas atoms [38, 39].

In addition to the effects associated with the electrostatic field, we also propose a significant electronic effect. As Ni contains an almost filled d-band, tunneling into Ni d-states is restricted to a small energy window up to 1 eV above the Fermi level in the spin minority channel - the spin majority d-band is completely filled even for charged surfaces. Ta, however, possesses a very high local density of unoccupied d-orbitals 0.5-3 eV above the Fermi level in both spin channels, as shown in Figure 3. Tunneling into these orbitals will further enhance the local ionization probability and hence the FIM brightness. We refrain from a quantitative analysis at this stage because tunneling into high-lying states is damped by the larger tunneling distance required to align the Ne level with the target state. Yet, we can assume that the brightest atoms

in the field-ion micrograph are hence Ta, while the others can be attributed to Ni (Figure 2(b)).

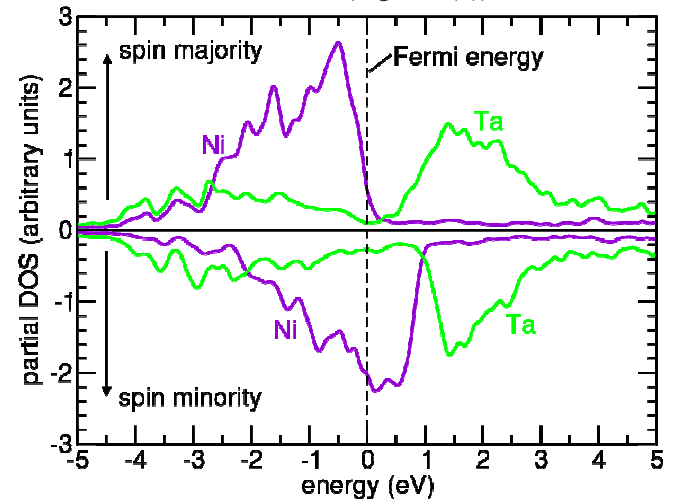


Figure 3: Partial density of states for a representative Ni atom and Ta in the top surface layer of a Ni (012) surface. Positive values correspond to spin majority, negative values to spin minority channel.

Experimentally, we studied the brightness contrast with AFIM. Figure 4(a) shows the recalculated FIM image, a two-dimensional histogram using 600000 successive detector impact positions. The (240) planes, delineated by the red square, were selected for the chemical identification as they exhibit an imaging resolution enabling the identification of individual atoms. As AFIM is operated at a pressure of  $10^{-6}$  mbar, the mass-to-charge spectrum was filtered using a similar protocol as Katnagallu et al. [16]. It uses the spatial correlations in the detection of Ne and Ni or Ne and Ta originating from the same high-voltage pulse. This protocol leads to the detection of  $\text{Ni}^{2+}$  ions shortly after the disappearance of the corresponding dimmer atom in the FIM image, shown in Figure 4(b). In comparison, the  $\text{Ta}^{3+}$  ion is detected immediately after the brighter atom's field evaporation, as shown in Figure 4(c).

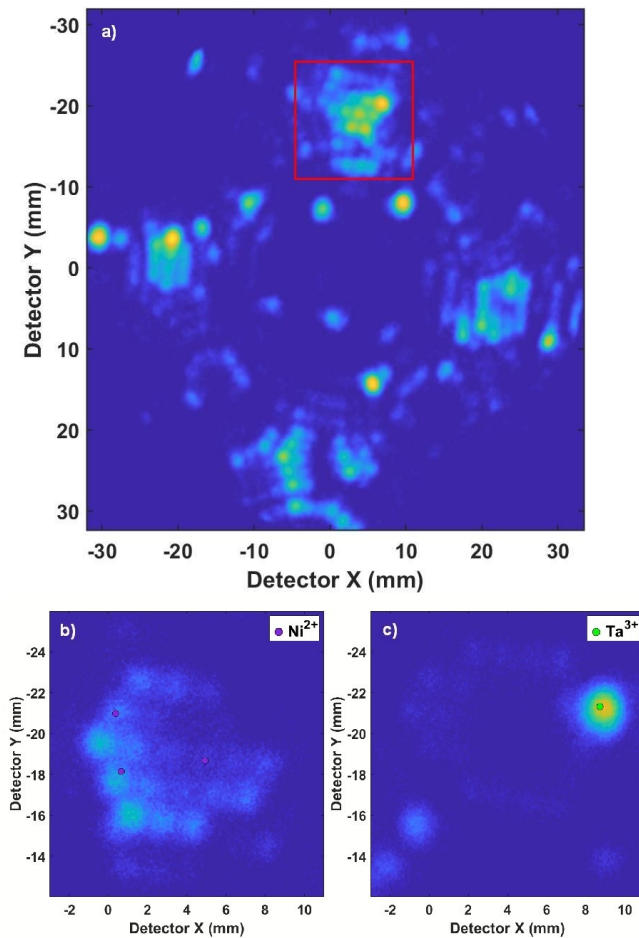


Figure 4: Analytical field ion microscopy measurement. (a) the field ion micrograph with the plane (240) highlighted. (b)-(c) shows the chemical mapping of  $\text{Ni}^{2+}$  and  $\text{Ta}^{3+}$  ions in the enlarged region.

In summary, we provide experimental confirmation for vacancy-Ta affinity through AFIM-DFT in a crept Ni-2 at.% Ta alloy. A random distribution of Ta in Ni is first revealed by a Ta-Ta nearest neighbor distance analysis of

the atom probe data. DFT calculations show that Ta atoms relax outwards compared to the surrounding Ni atoms and acquire higher electrical charges. We attribute the FIM contrast to a combination of electric and electronic factors: the charge induced local field enhances the local concentration of the gas and facilitates electron tunneling from the Ne imaging gas, which is further enhanced by the appearance of unoccupied Ta d-orbitals 1-3eV above the Fermi level. Meanwhile, the bright contrast of Ta solute in the Ni-matrix reveals a positive correlation between Ta solutes and vacancies. Our observations confirm the ab-initio results of Schuwalow et al. [31], who proposed attractive solute-vacancies interactions in Ni-Ta, in the first neighbor shell. It is also in agreement with the work reported by Pleiter and Hohenemser [40], which shows some positive correlation between vacancies and large atomic radius solutes. According to Ur Rehman et al. [30], the Ta solutes provide a more potent hardening than Re for lower temperatures. The binding of vacancies by the nearly homogeneously distributed Ta atoms within the Ni-matrix could potentially slow down dislocation climb processes [41, 42] involved in creep deformation. Hence, our results could suggest that other larger elements with positive binding energies to vacancies could further enhance superalloys' performance against creep deformation.

This work was supported by The International Max Planck Research School for Interface Controlled Materials for Energy Conversion (IMPRS-SurMat). We also appreciate the technical support of U. Tezins and A. Sturm at the APT/FIB facilities at Max-Planck-Institut für Eisenforschung. LTS & BG author acknowledges financial support from the ERC-CoG-SHINE-771602. The authors acknowledge funding by the Deutsche Forschungsgemeinschaft (DFG) through projects A4 and B3 of the collaborative research center SFB/TR 103 "From Atoms to Turbine Blades – a Scientific Approach for Developing the Next Generation of Single Crystal Superalloys".

\* f.ferraz@mpie.de

† b.gault@mpie.de

‡ l.stephenson@mpie.de

- [1] Q. Wu, W.-s. Miao, Y.-d. Zhang, H.-j. Gao and D. Hui, "Mechanical properties of nanomaterials: A review," *Nanotechnology Reviews*, vol. 9, pp. 259-273, 3 2020.
- [2] B. M. Jenkins, F. Danoix, M. Gouné, P. A. J. Bagot, Z. Peng, M. P. Moody and B. Gault, "Reflections on the Analysis of Interfaces and Grain Boundaries by Atom Probe Tomography," *Microscopy and Microanalysis*, vol. 26, p. 247–257, 2020.

- [3] A. Prakash, J. Guérolé, J. Wang, J. Müller, E. Spiecker, M. J. Mills, I. Povstugar, P. Choi, D. Raabe and E. Bitzek, "Atom probe informed simulations of dislocation–precipitate interactions reveal the importance of local interface curvature," *Acta Materialia*, vol. 92, pp. 33–45, 2015.
- [4] M. A. Puigví, N. de Diego, A. Serra, Y. N. Osetsky and D. J. Bacon, "On the interaction between a vacancy and self-interstitial atom clusters in metals," *Philosophical Magazine*, vol. 87, pp. 3501–3517, 2007.
- [5] E. W. Müller, "Resolution of the Atomic Structure of a Metal Surface by the Field Ion Microscope," *Journal of Applied Physics*, vol. 27, p. 474–476, 5 1956.
- [6] C. A. Speicher, W. T. Pimbley, M. J. Attardo, J. M. Galligan and S. S. Brenner, "Observation of vacancies in the field-ion microscope," *Physics Letters*, vol. 23, p. 194–196, 10 1966.
- [7] L. A. Beavan, R. M. Scanlan and D. N. Seidman, "The defect structure of depleted zones in irradiated tungsten," *Acta Metallurgica*, vol. 19, p. 1339–1350, 12 1971.
- [8] J. Y. Park, H. C. W. Huang, R. W. Siegel and R. W. Balluffi, "A quantitative study of vacancy defects in quenched tungsten by combined field-ion microscopy and electrical resistometry," *Philosophical Magazine A*, vol. 48, p. 397–419, 3 1983.
- [9] M. Dagan, B. Gault, G. D. W. Smith, P. A. J. Bagot and M. P. Moody, "Automated Atom-By-Atom Three-Dimensional (3D) Reconstruction of Field Ion Microscopy Data," *Microscopy and Microanalysis*, vol. 23, p. 255–268, 2017.
- [10] G. D. W. Smith, D. Hudson, P. D. Styman and C. A. Williams, "Studies of dislocations by field ion microscopy and atom probe tomography," *Philosophical Magazine*, vol. 93, p. 3726–3740, 9 2013.
- [11] H. B. Zeedijk, "Field-Ion Microscope Observation of Dislocations in Tungsten," *Journal of Applied Physics*, vol. 39, p. 5800–5802, 11 1968.
- [12] D. A. Smith and G. D. W. Smith, "Field ion microscopy," *Physics Bulletin*, vol. 21, p. 393–400, 9 1970.
- [13] R. J. Bayuzick and R. S. Goodrich, "Observations of grain boundaries with the field ion microscope," *Surface Science*, vol. 23, p. 225–239, 10 1970.
- [14] R. G. Forbes, "Seeing atoms: the origins of local contrast in field-ion images," *Journal of Physics D: Applied Physics*, vol. 18, p. 973–1018, 6 1985.
- [15] B. Klaes, R. Lardé, F. Delaroche, S. Parviainen, N. Rolland, S. Katnagallu, B. Gault and F. Vurpillot, "A model to predict image formation in the three-dimensional field ion microscope," *Computer Physics Communications*, p. 107317, 2020.
- [16] S. Katnagallu, L. T. Stephenson, I. Mouton, C. Freysoldt, A. P. A. Subramanyam, J. Jenke, A. N. Ladines, S. Neumeier, T. Hammerschmidt, R. Drautz, J. Neugebauer, F. Vurpillot, D. Raabe and B. Gault, "Imaging individual solute atoms at crystalline imperfections in metals," *New Journal of Physics*, vol. 21, p. 123020, 12 2019.
- [17] M. Perrut, P. Caron, M. Thomas and A. Couret, "High temperature materials for aerospace applications: Ni-based superalloys and  $\gamma$ -TiAl alloys," *Comptes Rendus Physique*, vol. 19, pp. 657–671, 2018.
- [18] H. Bian, X. Xu, Y. Li, Y. Koizumi, Z. Wang, M. Chen, K. Yamanaka and A. Chiba, "Regulating the coarsening of the  $\gamma'$  phase in superalloys," *NPG Asia Materials*, vol. 7, p. 212, 2015.
- [19] R. C. Reed, "Single-crystal superalloys for blade applications," in *The Superalloys: Fundamentals and Applications*, Cambridge University Press, 2006, p. 121–216.
- [20] T. M. Pollock and S. Tin, "Nickel-Based Superalloys for Advanced Turbine Engines: Chemistry, Microstructure and Properties," *Journal of Propulsion and Power*, vol. 22, pp. 361–374, 2006.
- [21] E. Alabort, D. Barba, S. Sulzer, M. Lißner, N. Petrinic and R. C. Reed, "Grain boundary properties of a nickel-based superalloy: Characterisation and modelling," *Acta Materialia*, vol. 151, pp. 377–394, 2018.
- [22] L. A. Jácome, P. Nörtershäuser, J.-K. Heyer, A. Lahni, J. Frenzel, A. Dlouhy, C. Somsen and G. Eggeler, "High-temperature and low-stress creep anisotropy of single-crystal superalloys," *Acta Materialia*, vol. 61, pp. 2926–2943, 2013.
- [23] R. C. Reed, "The Superalloys: Fundamentals and Applications," in *The Superalloys: Fundamentals and Applications*, Cambridge University Press, 2006, p. 1–32.
- [24] L. Cui, J. Yu, J. Liu, T. Jin and X. Sun, "The creep deformation mechanisms of a newly designed nickel-base superalloy," *Materials Science and Engineering: A*, vol. 710, pp. 309–317, 2018.
- [25] A. P. Mouritz, "Creep of aerospace materials," in *Introduction to Aerospace Materials*, Elsevier, 2012, p. 521–533.
- [26] S. D. Mesarovic, "Dislocation Creep: Climb and Glide in the Lattice Continuum," *Crystals*, vol. 7, p. 243, 8 2017.
- [27] S. Giese, A. Bezold, M. Pröbstle, A. Heckl, S. Neumeier and M. Göken, "The Importance of Diffusivity and Partitioning Behavior of Solid Solution Strengthening Elements for the High Temperature Creep Strength of Ni-Base Superalloys," *Metallurgical and Materials*

*Transactions A*, 10 2020.

- [28] A. Mottura and R. C. Reed, "What is the role of rhenium in single crystal superalloys?," *MATEC Web of Conferences*, vol. 14, p. 01001, 2014.
- [29] X. Wu, S. K. Makineni, C. H. Liebscher, G. Dehm, J. R. Mianroodi, P. Shanthraj, B. Svendsen, D. Bürger, G. Eggeler, D. Raabe and B. Gault, "Unveiling the Re effect in Ni-based single crystal superalloys," *Nature Communications*, vol. 11, 1 2020.
- [30] H. U. Rehman, K. Durst, S. Neumeier, A. Sato, R. Reed and M. Göken, "On the temperature dependent strengthening of nickel by transition metal solutes," *Acta Materialia*, vol. 137, pp. 54-63, 2017.
- [31] S. Schuwalow, J. Rogal and R. Drautz, "Vacancy mobility and interaction with transition metal solutes in Ni," *Journal of Physics: Condensed Matter*, vol. 26, p. 485014, 11 2014.
- [32] B. Gault, A. J. Breen, Y. Chang, J. He, E. A. Jäggle, P. Kontis, P. Kürsteiner, A. Kwiatkowski da Silva, S. K. Makineni, I. Mouton and et al., "Interfaces and defect composition at the near-atomic scale through atom probe tomography investigations," *Journal of Materials Research*, vol. 33, p. 4018-4030, 2018.
- [33] L. T. Stephenson, M. P. Moody, P. V. Liddicoat and S. P. Ringer, "New Techniques for the Analysis of Fine-Scaled Clustering Phenomena within Atom Probe Tomography (APT) Data," *Microscopy and Microanalysis*, vol. 13, p. 448-463, 2007.
- [34] A. Metsue, A. Oudriss, J. Bouhattate and X. Feugas, "Contribution of the entropy on the thermodynamic equilibrium of vacancies in nickel," *The Journal of Chemical Physics*, vol. 140, no. 10, p. 104705, 2014.
- [35] K. Stiller and H.-O. Andren, "Faulty field evaporation at di-vacancies in  $\text{W}$  tungsten," *Surface Science*, vol. 114, p. L57-L61, 2 1982.
- [36] S. Boeck, C. Freysoldt, A. Dick, L. Ismer and J. Neugebauer, "The object-oriented DFT program library S/PHI/nX," *Comp. Phys. Comm.*, vol. 182, pp. 543-554, 2011.
- [37] C. Freysoldt, A. Mishra, M. Ashton and J. Neugebauer, "Generalized dipole correction for charged surfaces in the repeated-slab approach," *Physical Review B*, vol. 102, p. 045403, 7 2020.
- [38] R. G. Forbes, H. J. J. Kreuzer and R. L. C. L. C. Wang, "On the theory of helium field adsorption," *Applied Surface Science*, Vols. 94-5, p. 60-67, 3 1996.
- [39] R. L. C. Wang, H. J. Kreuzer and R. G. Forbes, "Field adsorption of helium and neon on metals: An integrated theory," *Surface Science*, vol. 350, p. 183-205, 1996.
- [40] F. Pleiter and C. Hohenemser, "Interpretation of vacancy migration, trapping, and clustering in fcc metals as observed through perturbed angular correlations and distributions of  $\gamma$ -rays," *Phys. Rev. B*, vol. 25, no. 1, pp. 106-126, 1982
- [41] H. Yang, M. Huang and Z. Li, "The influence of vacancies diffusion-induced dislocation climb on the creep and plasticity behaviors of nickel-based single crystal superalloy," *Computational Materials Science*, vol. 99, p. 348-360, 3 2015.
- [42] M. Lenz, M. Wu and E. Spiecker, "Segregation-assisted climb of Frank partial dislocations: An alternative route to superintrinsic stacking faults in L12-hardened superalloys," *Acta Materialia*, vol. 191, p. 270-279, 6 2020.